BIG – Branschsamverkan i grunden

Forskningsprogram för effektiv och säker grundläggning av vägar och järnvägar

Projekt A2019:02

Degradation of a natural sensitive clay under cyclic loading

Final Report

CHALMERS UNIVERSITY OF TECHNOLOGY

KTH

TRAFIKVERKET

STATENS GEOTEKNISKA INSTITUT

LULEÅ TEKNISKA UNIVERSITET

BIG – Branschsamverkan i grunden
Forskningsprogram för effektiv och säker grundläggning av vägar och järnvägar

Rapport BIG projekt A2019:02

Degradation of a natural sensitive clay under cyclic loading

Final report

Jelke Dijkstra, Hossein Tahershamsi, Reza Ahmadi Naghdeh

Framtagen inom ramen för BIG av Chalmers Tekniska Högskola

Stockholm 2022

Rapport publicerad av BIG, Branschsamverkan i grunden
Beställning Web: www.big-geo.se

ISBN 978-91-986927-0-9
Upplaga Digital

Framtagen av Chalmers Tekniska Högskola
Department of Architecture and Civil Engineering
Geology & Geotechnics
Författare Jelke Dijkstra, Hossein Tahershamsi, Reza Ahmadi Naghdeh



CHALMERS

A2019-02 - Degradation of a natural sensitive clay under cyclic loading

JELKE DIJKSTRA, HOSSEIN TAHERSHAMSI & REZA AHMADI NAGHADEH

Department of Architecture & Civil Engineering
Geology & Geotechnics
CHALMERS UNIVERSITY OF TECHNOLOGY
Göteborg, Sweden 2022

TECHNICAL REPORT

A2019-02 - Degradation of a natural sensitive clay under cyclic loading

JELKE DIJKSTRA, HOSSEIN TAHERSHAMSI & REZA AHMADI NAGHADEH

Department of Architecture & Civil Engineering
Geology & Geotechnics
CHALMERS UNIVERSITY OF TECHNOLOGY
Göteborg, Sweden 2022

A2019-02 - Degradation of a natural sensitive clay under cyclic loading
JELKE DIJKSTRA, HOSSEIN TAHERSHAMSI & REZA AHMADI NAGHADEH

© JELKE DIJKSTRA, HOSSEIN TAHERSHAMSI & REZA AHMADI NAGHADEH, 2022

Technical report A2019-02
ISSN n/a
Department of Architecture & Civil Engineering
Geology & Geotechnics
Chalmers University of Technology
SE-412 96 Göteborg
Sweden

Göteborg, Sweden 2022

A2019-02 - Degradation of a natural sensitive clay under cyclic loading
Technical report
JELKE DIJKSTRA, HOSSEIN TAHERSHAMSI & REZA AHMADI NAGHADEH
Department of Architecture & Civil Engineering
Geology & Geotechnics
Chalmers University of Technology

Abstract

This report summarises the advances made at Chalmers on modelling and testing natural soft soils that are quasi-statically loaded with cyclic stress paths, with a focus on the evolution of stiffness and damping ratio with the number of loading cycles. As such, the findings are directly applied in follow-up projects funded by Trafikverket, FORMAS, and CHARMEC. The main deliverable include the extension of a rate-dependent effective stress based constitutive model to incorporate strain accumulation and small-strain stiffness degradation for natural soft soils. This model in its generalised form can be incorporated in a commercial finite element program, as a user-defined model that is available for other scientists and engineers. The recently developed software and hardware for cyclic triaxial testing of soft soils using a Bishop-Wesley cell and local instrumentation, in combination with the new temperature-controlled GEO laboratory at Chalmers, has subsequently been used to determine the evolution of stiffness and damping as number of load cycles. In addition, the effect of loading amplitude and pre-shearing have been studied.

Keywords: Stiffness degradation, cyclic loading, natural clay, constitutive modelling, laboratory tests

Contents

Abstract **i**

Contents **iii**

1 Introduction **1**
1.1 Background 1
1.2 Aim and objectives 1
1.3 Limitations and changes along the way 2

2 Cyclic accumulation model for soft soils **3**
2.1 Creep-SCLAY1Sc model 3
2.2 Small-strain stiffness 4

3 Cyclic triaxial tests **5**
3.1 Test setup 5
3.2 Test programme 5
3.3 Test Results 9
3.3.1 Consolidation stage 10
3.3.2 Secant stiffness E^u_{sec} 11
3.3.3 Damping ratio 14
3.3.4 Post-cyclic shearing 16
3.3.5 Discussion of results 17

4 Conclusions, recommendations & impact **19**
4.1 Conclusions 19
4.2 Recommendations 20
4.3 Impact 20

References **21**

1 Introduction

1.1 Background

In many situations, a previously adequate railway track foundation starts to emit stronger than expected ground vibrations in the soil, and the existing vibration mitigating solutions become inadequate. The subsoil is the most persistent source of these issues, as track and subgrade related causes can be addressed during maintenance cycles. Furthermore, these track components are engineered for their function. Over the lifetime of the railway structure the dynamic soil properties, especially in weakly bonded soft soils such as those in the Nordic countries, will change. Here, the dynamic soil properties are those that affect the inertial response of the soil, *i*.e., mass, damping & stiffness. The unfavourable change of the latter two soil properties due to (repeated, dynamic) loading is considered degradation. The consolidation and creep, resulting from the permanent load induced by the self-weight of the railway structure, will induce delayed settlements of the system and non-stationary excess porewater pressures, which in turn will lead to a change in dynamic soil properties. Furthermore, the deviatoric stress in the soil below the railway system will increase, this so-called pre-shearing will have an impact on the subsequent resilience against cyclic loading. Prior research (Powrie et al., 2019; Dijkstra and Tahershamsi, 2020a) has shown that for a point in the soil below the embankment only low frequencies are of importance. As a result, for events with a low loading amplitude the acceleration, hence the inertial component, is low (Wichtmann, 2005). This implies that a non-monotonic quasi-static loading drives the degradation in the soil below the subgrade and embankment. In contrast, for wave propagation problems, such as train induced vibrations the dynamic properties are still of concern. Therefore, it is prudent to the study the impact of cyclic loading on the evolving stiffness and damping of a natural Swedish soft clay. The following research questions are formulated:

- How will cyclic loading affect the slow processes of consolidation and creep in soft soils and the resulting accumulated irreversible deformations?
- What is the effect of complex loading history on the dynamic soil properties, such as stiffness, as function of strain amplitude and strain rate and material damping?

The first research question has been addressed in previous projects, *i*.e., BIG projects A2016-05 and A2017-07, where respectively a cyclic accumulation model for soft soils has been developed (Dijkstra and Tahershamsi, 2020b; Zuada Coelho et al., 2021) and subsequently used to study a transition zone (Dijkstra and Tahershamsi, 2020a). In those projects, however, there was no experimental evidence for Swedish sensitive clay, as well as that the impact of cyclic loading on dynamic properties was not explicitly considered. As a result, a small-strain formulation for the stiffness evolution in the model was absent, yet deemed crucial. Similarly, the initiation of cyclic triaxial testing at Chalmers as reported in Karstunen and Dijkstra (2021) needed further developments to extract the data required.

1.2 Aim and objectives

The aim of the project was to study the interplay between cyclic loading and the emerging dynamic soil properties, *i*.e., stiffness & damping, in a sensitive soft soil.

The objectives of the project were the following:

- Triaxial testing of high-quality samples of soft clay under cyclic loading with a focus on small and large loading amplitudes, as well as pre-shearing;
- Extension of cyclic accumulation model for small strain;

1.3 Limitations and changes along the way

Early in the project we realised that the cyclic-accumulation model developed in previous projects needed to be extended for small strains, which required more extensive laboratory testing than those already available, that in turn required evaluating local instrumentation for the Bishop-Wesley cells at Chalmers as well as a modification of the Creep-SCLAY1Sc.

2 Cyclic accumulation model for soft soils

2.1 Creep-SCLAY1Sc model

The Creep-SCLAY1Sc model is an extension of Creep-SCLAY1S, *i*.e., developed for cyclic loading (Zuada Coelho et al., 2021). As such it inherits all the features from Creep-SCLAY1S. The accumulation of irreversible strain from cyclic loading is captured with an additional component of viscoplastic strain, using a second cumulative viscoplastic multiplier. Therefore, Creep-SCLAY1Sc is considered to be an explicit model (the strain from cyclic loading is directly calculated) for cyclic loading that captures the long-term response of natural clays under cyclic loading conditions.

The constitutive model follows a similar strain decomposition as the original Creep-SCLAY1S, except for the inclusion of a cyclic component in the viscoplastic strain tensor:

$$\dot{\boldsymbol{\epsilon}} = \dot{\boldsymbol{\epsilon}}^{e} + \underbrace{(\dot{\boldsymbol{\epsilon}}^{c} + \dot{\boldsymbol{\epsilon}}^{cyc})}_{\dot{\boldsymbol{\epsilon}}^{vp}} \tag{2.1}$$

where in eq. (2.1):

$\dot{\boldsymbol{\epsilon}}^{e}$ = elastic strain rate
$\dot{\boldsymbol{\epsilon}}^{vp}$ = viscoplastic strain rate
$\dot{\boldsymbol{\epsilon}}^{c}$ = creep strain rate
$\dot{\boldsymbol{\epsilon}}^{cyc}$ = cyclic strain rate

The associated flow rule remains the same as the original Creep-SCLAY1S, however, with an additional viscoplastic multiplier $\dot{\Omega}$ that captures the cyclic accumulation. Thus, the viscoplastic component of eq. (2.1) becomes:

$$\dot{\boldsymbol{\epsilon}}^{vp} = [\dot{\Omega} + \dot{\Lambda}]\frac{\partial p'_{eq}}{\partial \boldsymbol{\sigma}'} \tag{2.2}$$

The cyclic viscoplastic multiplier is derived using laboratory data on Onsøy clay under undrained cyclic triaxial loading at different loading amplitudes and periods (Wichtmann et al., 2013). The proposed eq. (2.3) contains three normalised terms: term *i* represents the gradient of the cyclic axial strain; term *ii* controls the frequency dependency of the model; and term *iii* captures the loading amplitude dependence.

$$\dot{\Omega} = \underbrace{\frac{\zeta}{t_{\text{ref}|0.1\%}}}_{i}\underbrace{\left(\frac{T}{T_0}\right)^{\Xi}}_{ii}\underbrace{\left(\frac{q_{\text{cyc}}}{p'M(\theta) - q}\right)^{\iota}}_{iii} \tag{2.3}$$

The cyclic reference time at 0.1% of deviatoric strain, $t_{\text{ref}|0.1\%}$, is defined in eq. (2.4):

$$t_{\text{ref}|0.1\%} = \Gamma_{\alpha}\left(\frac{q_{\text{cyc}}}{p'_0}\right)^{-\Gamma_{\beta}} \tag{2.4}$$

T_0 and T in eq. (2.3) denote the reference and current loading period, respectively. q_{cyc} is the cyclic deviatoric stress, $M(\theta)$ the critical state stress ratio, p' the current mean effective stress, and q is the current deviatoric stress. Moreover, p'_0 stated in eq. (2.4) is the initial mean

effective stress. In conclusion, the cyclic viscoplastic multiplier introduces five more parameters when compared to Creep-SCLAY1S, in which:

- ζ: Axial strain accumulation factor in [d]; controls the gradient of the cyclic strain (*i*.e., measured at reference time $t_{\mathrm{ref}|0.1\%}$)
- Γ_α: scaling factor of cyclic reference time
- Γ_β: exponential scaling factor of cyclic reference time
- Ξ: scaling factor of loading period
- ι: scaling factor for the fraction of cyclic and static loading

2.2 Small-strain stiffness

As part of the implementation of the constitutive model in a Finite Element framework an elastic stiffness matrix K_{ijhk} that is dependent on the mean effective stress p' is assembled. Basically, a 6x6 stiffness matrix following Hooke's law, where the elastic stiffness in the overconsolidated region $\kappa^\star$ and the Poisson ratio ν of Creep-SCLAY1S or Creep-SCLAY1Sc are used to calculate the shear modulus G, and subsequently the components of K_{ijhk}.

$$G = \frac{3p'(1-2\nu)}{2\kappa^\star(1+\nu)} \tag{2.5}$$

resulting in D_{ijhk} (index notation used, with Kronecker delta δ):

$$K_{ijhk} = \frac{2G\nu}{1-2\nu}\delta_{ij}\delta_{hk} + G(\delta_{ik}\delta_{jh} + \delta_{ih}\delta_{jk}) \tag{2.6}$$

The small-strain extension simply replaces G with an expression that depends on the strain history, and the highest attainable stiffness at small strain $G_{max} = G_0$. Here, we follow a suggestion by Sivasithamparam et al. (2021), *i*.e.,

$$G = G_0\left[1 - \frac{\langle \varepsilon_q - \varepsilon_s \rangle}{A + B\langle \varepsilon_q - \varepsilon_s \rangle}\right] \tag{2.7}$$

where G_0 is the reference stiffness at small strain, which remains a function of the mean effective stress p' that will be reduced towards a limiting value that is controlled by parameters A and B and the shear strain history. The deviatoric component of the total strain ε_q is compared to a threshold value ε_s, which is set internally at 10^{-5}. $\langle . \rangle$ are Macaulay brackets that return $(\varepsilon_q - \varepsilon_s)$ for $(\varepsilon_q - \varepsilon_s) > 0$ and 0 otherwise. It would be logical to choose values for A and B, such that G ranges between G_0 and G at engineering strain levels. Additionally, this relation might be affected by further degradation of both G_0 and G that results from cyclic loading. The latter will be studied experimentally in the following Chapter.

3 Cyclic triaxial tests

The following provides an overview of the cyclic triaxial tests performed to quantify the effect of cyclic loading on the degradation of the (secant) undrained stiffness and the damping. Compared to prior tests reported in Karstunen and Dijkstra (2021), a more systematic test series has been performed that investigates the impact of loading amplitude and pre-shearing on the subsequent response.

3.1 Test setup

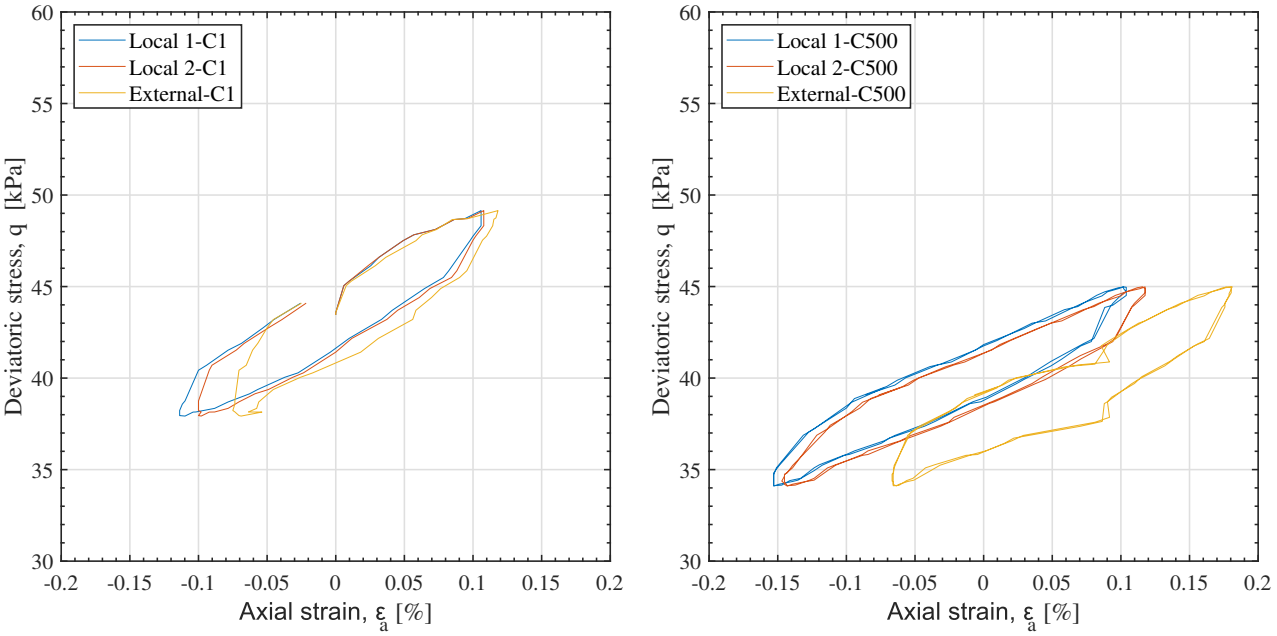
A conventional computer-controlled Bishop and Wesley (1975) type hydraulic stress path apparatus, equipped with submersible internal load cells, was modified to perform cyclic loading tests on 50 mm diameter, 100 mm high, specimens. External LVDT transducers were used to measure the axial strains. In some of the tests local instrumentation, comprising of two submersible transducers mounted to the mid section of the sample, was employed.

Figure 3.1 shows that the external instrumentation tracks the local instrumentation well (Figure 3.1a), *i*.e., the subsequent derivation of the secant stiffness and the damping ratio is of high quality. For the local instrumentation some problems were encountered. As shown in the comparison in Figure 3.1b, the magnitude of the total accumulated strain is permanently shifted as the number of loading cycles increases. After inspection it was concluded that the instrumentation was not securely mounted, *i*.e., due to a weakening membrane from the paraffin oil in the cell, the local instrumentation sagged. As an example after 500 stress loops, the data from the local sensor data is shifted on the strain axis (horizontal) when compared to the external measurements (Fig. 3.1b). The magnitude of the damping and stiffness, however, still is well tracked by both forms of instrumentation. Hence, for the purpose of this report all stiffness and damping data is considered of similar quality. Only test 5 showed somewhat unreliable interpretation of the stiffness, although the strain levels in this test were higher than the other tests executed with this stress amplitude.

Porewater pressures were measured at the base of the specimen. The cyclic load was applied with a sufficiently low rate (period of 180 s) to allow tracking of the changes in the porewater pressures during undrained monotonic shearing or cyclic loading stage. A suction cap was employed to enable to perform cyclic loading towards the extension regime and to centralise the applied load between the load cell and top platen. In the presented test series GDS controllers were used to control cell, back and ram pressure during the consolidation, undrained pre-shearing and cyclic loading stages. The GDS equipment was controlled using GDSlab. Although the Cetoni syringe pump system has superior control accuracy, the GDS system is somewhat better suited for testing larger samples volumes over a long period of time.

3.2 Test programme

A total of eleven carefully planned monotonic (3) and cyclic (8) undrained triaxial tests, listed in Table 3.1 were performed on high-quality cylindrical undisturbed samples taken from 7 to 9 m depth, from the new Chalmers test site near Kärra in Gothenburg. After assessing the monotonic results (Anisotropically Consolidated undrained test sheared in compression - CAUC) only samples from 9 m depth were used for the cyclic tests.



(a) *First cycle* (b) *500th cycle*

Figure 3.1: *Comparison of local (Local 1 and Local 2; one sensor on each side of the sample) vs. external instrumentation during cyclic triaxial test. Note the shift of the strain loop for the local instrumentation which is linked to membrane softening.*

The systematic testing of samples from a single depth enables isolating the impact of pre-shearing and loading amplitude on the results. The depth of the water table is close to the ground surface at this site. Hence, the *in-situ* stress state corresponds to a mean effective stress p'_0 of 42 kPa and a deviatoric stress q_0 of 28 kPa. The testing programme is intended to provide information that is most relevant to cyclic loading related to high-speed (HS) railway lines, such as those planned in Sweden. Cyclic loading was defined by three loading components:

1. the aforementioned *in-situ* deviatoric stress q_0, which was applied slowly as part of the consolidation stage;

2. an optional undrained pre-shearing with amplitude q_p (loading or unloading) which sums up to the mean deviator stress q_{mean};

3. the undrained cyclic loading amplitude q_{cyc} is subsequently superimposed on the q_{mean}. However, $q_{mean} + q_{cyc} < q_{max}$, where the maximum deviator stress equals two times the undrained shear strength: $q_{max} = 2s_u$. The undrained shear strength is determined from the monotonic tests as $s_u = 66$ kPa .

As such the complete test was stress controlled, whereas the emerging (accumulated) strains and (excess) porewater pressures are measured during the test.

An overview of the loading programme in q_{mean} - q_{cyc} space is shown in Figure 3.2. Note that two data series can be identified: in the first series the mean stress q_{mean} is kept constant and the impact of cyclic loading amplitude q_{cyc} will be studied, whereas in the second series with pre-shearing the q_{mean} is increased or reduced whilst appropriating changing q_{cyc} to preserve a comparable stability (safety) factor FS compared to the test that is anisotropically consolidated to *in-situ* conditions.

An average test duration of 21 days is required to first consolidate the sample anisotropically, and subsequently apply 10 000 load cycles. As can be seen from Table 3.1 some tests were allowed to continue up to 45 000 loading cycles (total test duration of 3 months), whereas other tests were aborted prematurely and subsequently sheared to failure in undrained conditions.

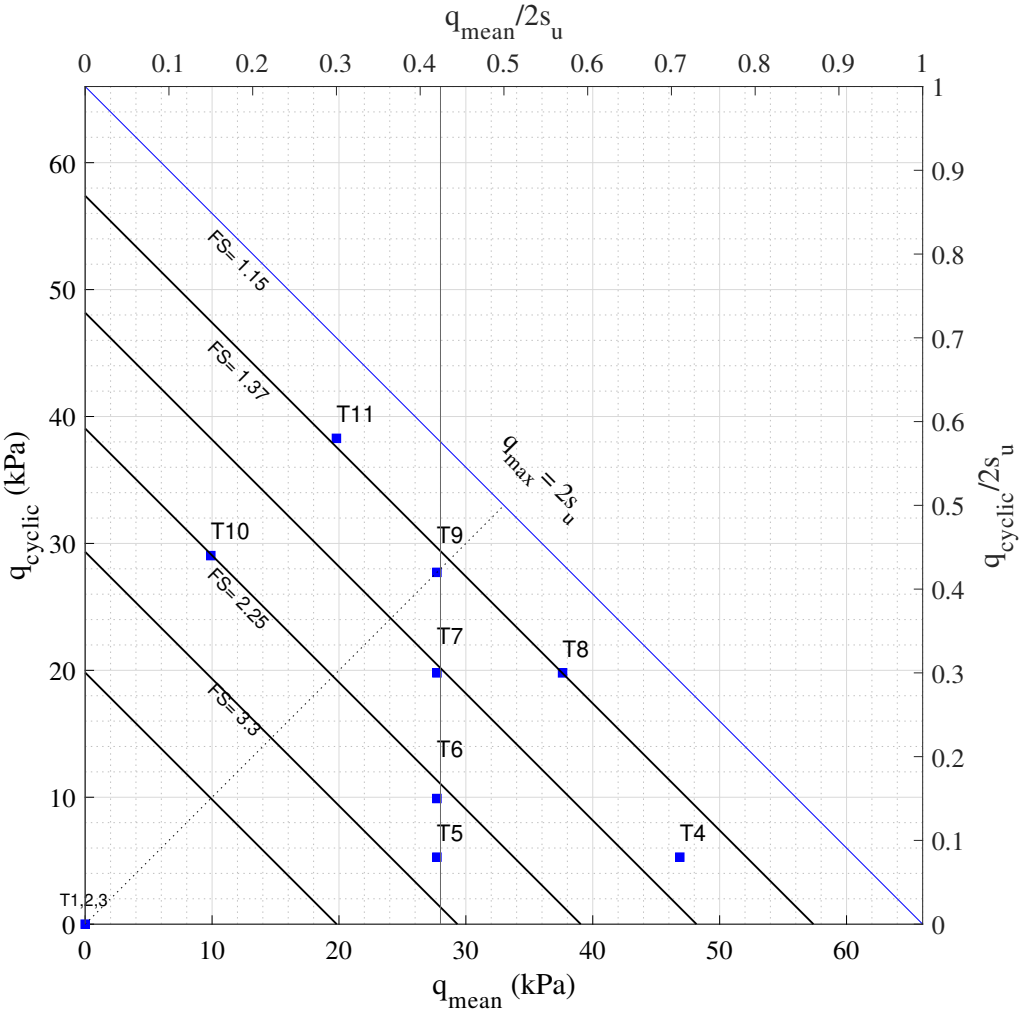


Figure 3.2: *Test overview for cyclic triaxial tests on a samples from* 9 m *depth. Note that* q_{mean} = 28 kPa *corresponds to the in-situ deviatoric stress level* q_0 *and that for all tests* p'_0 *is* 42 kPa.

No.	Test Name	q_0 (kPa)	p'_0 (kPa)	q_m (kPa)	q_p (kPa)	$q_m/2s_u$	q_{cyc} (kPa)	$q_{cyc}/2s_u$	Status		N_f
1	Test 01 (9m)	28	42	-	-	-	0 (Mon)	-	Completed	F	-
2	Test 02 (8m)	25	42	-	-	-	0 (Mon)	-	Completed	F	-
3	Test 03 (7m)	22	42	-	-	-	0 (Mon)	-	Completed	F	-
4	Test 04	28	42	47	19	0.71	5	0.076	Completed	PCF	-
5	Test 05	28	42	28	0	0.42	5	0.076	Completed	PCF	-
6	Test 06	28	42	28	0	0.42	10	0.15	Completed	PCF	-
7	Test 07	28	42	28	0	0.42	20	0.3	Completed	CF	$\tilde{}$5000
8	Test 08	28	42	37	9	0.56	20	0.3	Completed	CF	580
9	Test 09	28	42	28	0	0.42	28	0.42	Completed	CF	5800
10	Test 10	28	42	10	-18	0.15	29	0.44	Completed	CF	9000
11	Test 11	28	42	20	-8	0.3	38	0.58	Completed	CF	70

Table 3.1: Summary of undrained monotonic and cyclic triaxial test conditions for Kärra clay.

3.3 Test Results

In the following we will focus on the evolution of two main components as function of the number of loading cycles: (i) the secant (undrained) Young modulus E^u_{sec} of the cyclic loading loop and (ii) the material damping ratio D which is interpreted as the normalised area enclosed by the cyclic loop A_L, normalised by the total amount of work (the area A_T below the loop). See Figure 3.3. Both are evaluated from the raw cyclic triaxial data and plotted as function of the number of loading cycles N.

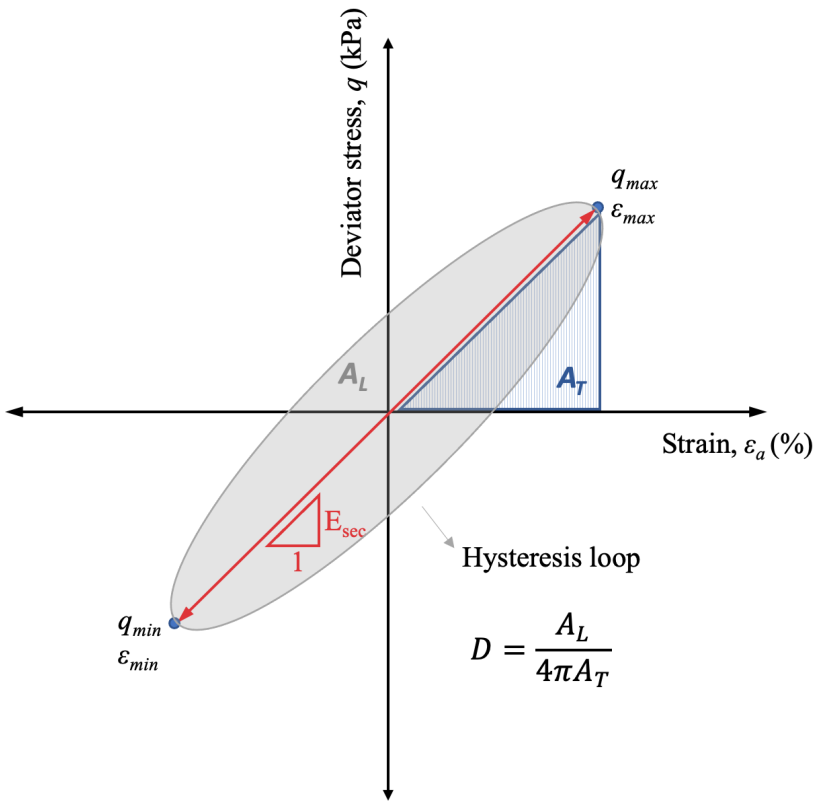


Figure 3.3: *Interpretation of E^u_{sec} and damping ratio D from cyclic triaxial data.*

The test results are presented first in Sections 3.3.1 – 3.3.4 before being discussed in more detail in Section 3.3.5.

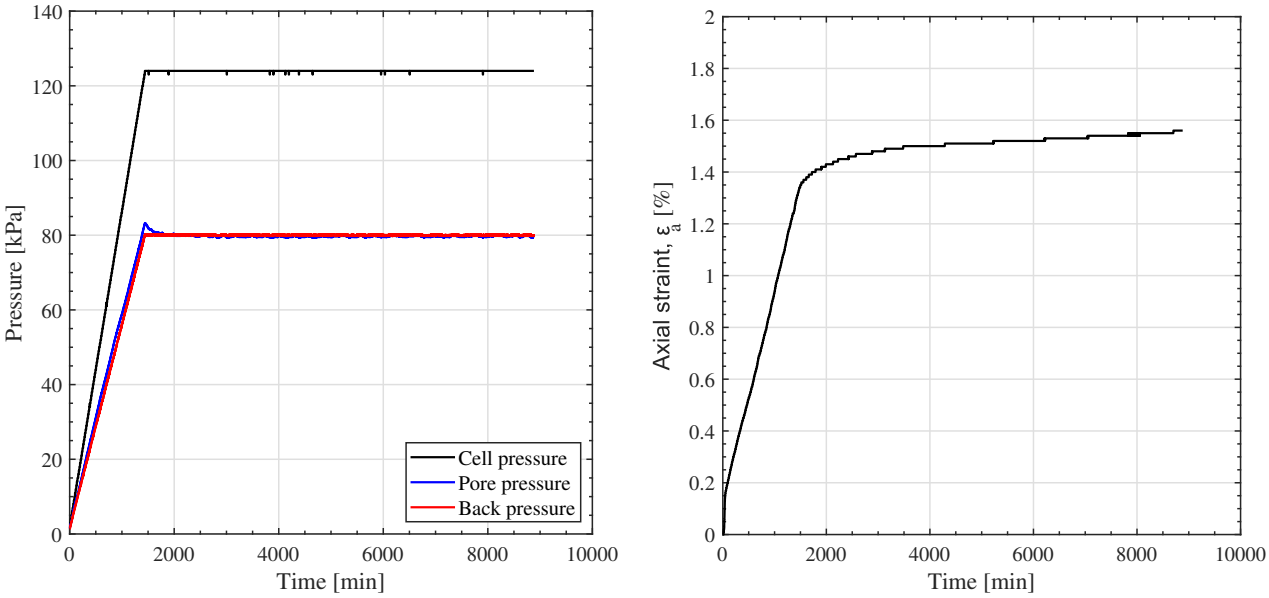
A distinction is made between the four tests wihout pre-shearing (tests 05, 06, 07 & 09), *i*.e., the tests that are immediately loaded after being anisotropically consolidated to the *in-situ* conditions (Figs. 3.5 & 3.8) and the tests that were pre-sheared prior to cyclic loading (tests 04, 08, 10 & 11 shown in Figs. 3.6 & 3.9). The main motivation for this loading protocol is to capture the effect of pre-loading resulting from, *e*.g., embankment construction and or an excavation.

Three of the tests, executed with a small cyclic loading amplitude, did not fail during the cyclic loading stage, *i*.e., tests 07, 04, 05, 06. Those tests where sheared to failure in undrained conditions as reported on in Section 3.3.4. See Table 3.1 for all test details.

3.3.1 Consolidation stage

For the current investigation, the on-going strain at the end of consolidation potentially should be factored in the interpretation of the accumulated cyclic strain. The on-going axial strain rate at the end of the (anisotropic) consolidation stage is rather large for samples that are consolidated to *in-situ* conditions. In one of the tests this creep stage was extended for several days, to investigate any tapering of the strain rate.

As shown in Figure 3.4a, the generation and dissipation of excess pore pressures during the consolidation stage are finished at around 2000 min, after which the axial strain continues to increase with $\approx 0.02\,\%\,\mathrm{d}^{-1}$ (Figure 3.4b). This on-going trend does not affect the interpretation of the secant undrained stiffness or damping ratio. In contrast, the accumulated axial strain should be corrected for this creep strain rate, in case the cyclic accumulation needs to be inferred independently. However, when calibrating the cyclic accumulation model the accumulation of the total viscoplastic strain, *i*.e., creep and cyclic accumulation should be sufficient.



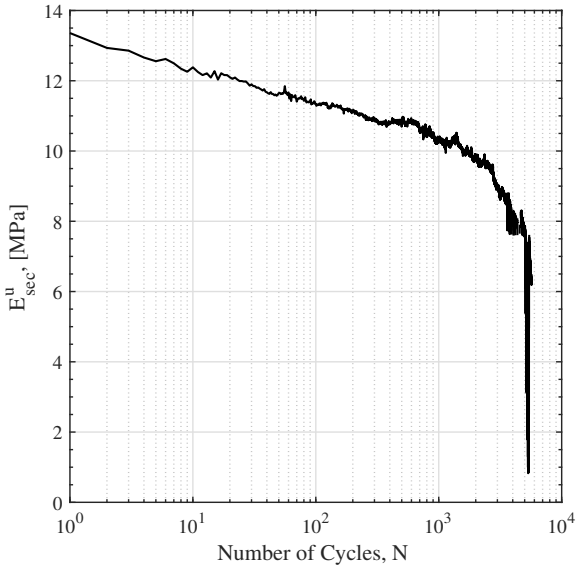
(a) *Cell, back and pore pressures.* (b) *Axial strain* ε_a.

Figure 3.4: *Cell and back pressure applied to the sample during consolidation (controlled) and emerging pore pressures and axial strain (measured).*

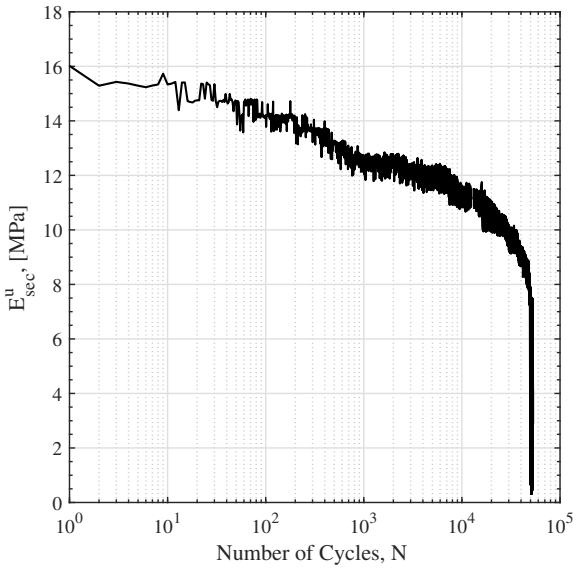
3.3.2 Secant stiffness E^u_{sec}

Without pre-shearing

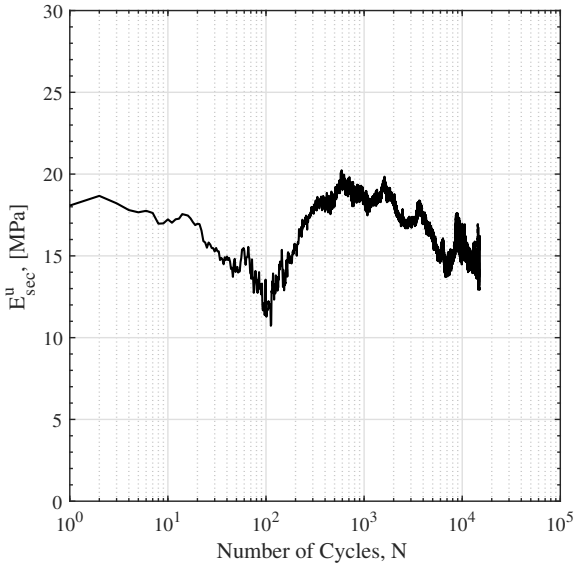
Fig. 3.5 presents the evolution of E^u_{sec} as function of the number of loading cycles N for samples without undrained pre-shearing. The results are organised as function of cyclic loading amplitude q_{cyc}, starting with $q_{cyc} = 28\,\text{kPa}$ and $q_{cyc} = 20\,\text{kPa}$ in Figs. 3.5a & 3.5b that ultimately led to failure after respectively 5800 and 45000 loading cycles. Subsequently, two tests loaded with substantially smaller loading amplitudes at $q_{cyc} = 10\,\text{kPa}$ and $q_{cyc} = 5\,\text{kPa}$, shown in Figs. 3.5c & 3.5d did not reach failure.



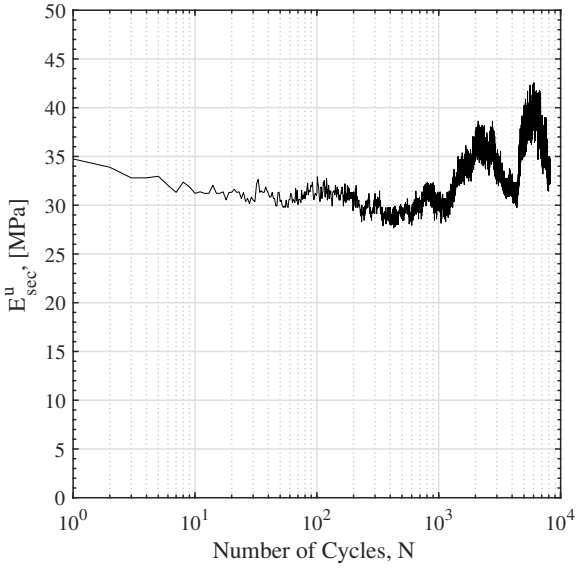
(a) $q_{mean} = 28\,\text{kPa}$; $q_{cyc} = 28\,\text{kPa}$



(b) $q_{mean} = 28\,\text{kPa}$; $q_{cyc} = 20\,\text{kPa}$



(c) $q_{mean} = 28\,\text{kPa}$; $q_{cyc} = 10\,\text{kPa}$

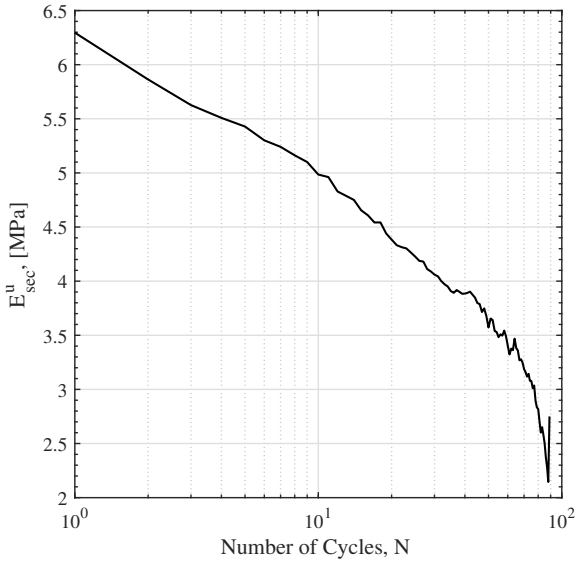


(d) $q_{mean} = 28\,\text{kPa}$; $q_{cyc} = 5\,\text{kPa}$

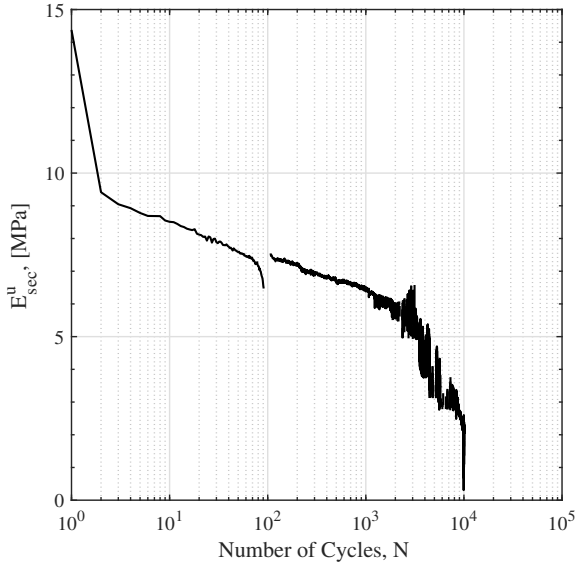
Figure 3.5: *Evolution of undrained secant Young modulus E^u_{sec} as function of the number of loading cycles N for cyclic triaxial tests that are anisotropically consolidated to* in-situ *stress conditions p'_0, q_0 before undrained cyclic loading with q_{cyc}. Note that the tests with $q_{cyc} = 5$ & 10 kPa did not fail during cyclic loading.*

With pre-shearing

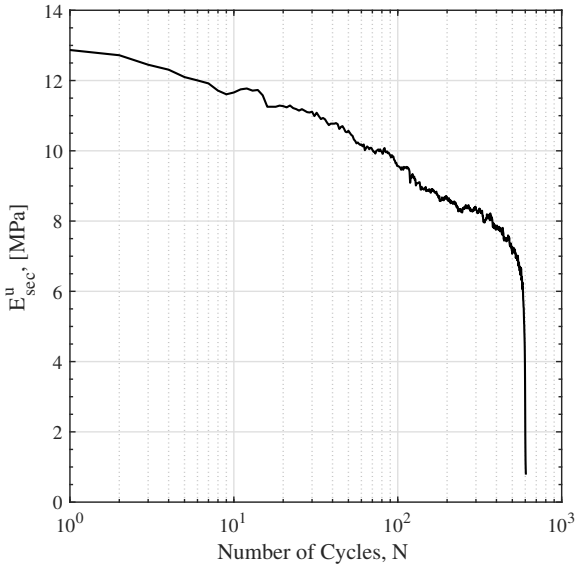
Fig. 3.6 presents the evolution of E^u_{sec} as function of N for samples without undrained pre-shearing. Figs. 3.6a & 3.6b were first unloaded to respectively $q_{mean} = 20\,\text{kPa}$ and $q_{cyc} = 10\,\text{kPa}$ before cyclically loaded with $q_{cyc} = 38\,\text{kPa}$ and $q_{cyc} = 28\,\text{kPa}$. Figs. 3.6c & 3.6d, on the other hand, were pre-sheared in compression before loaded with a cyclic loading amplitude of $q_{cyc} = 20\,\text{kPa}$ and $q_{cyc} = 5\,\text{kPa}$. With exception of one test ($q_{cyc} = 5\,\text{kPa}$), all tests failed rather quickly after respectively $N = 70$, 9000 and 580 loading cycles (Figs. 3.6a, 3.6b & 3.6c).



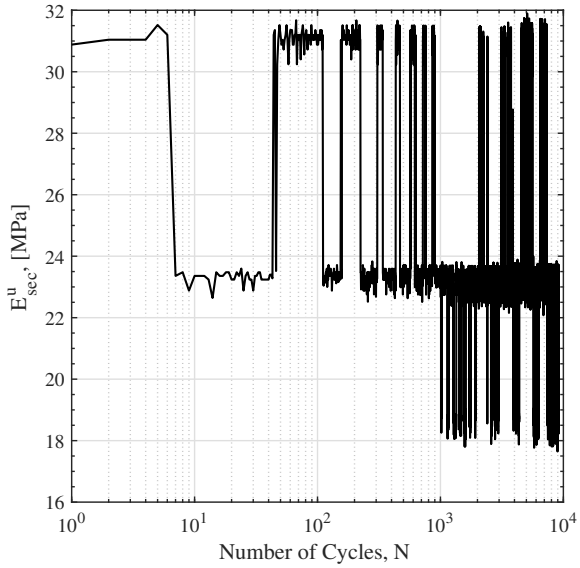
(a) $q_{mean} = 20\,\text{kPa}$; $q_{cyc} = 38\,\text{kPa}$



(b) $q_{mean} = 10\,\text{kPa}$; $q_{cyc} = 29\,\text{kPa}$



(c) $q_{mean} = 37\,\text{kPa}$; $q_{cyc} = 20\,\text{kPa}$

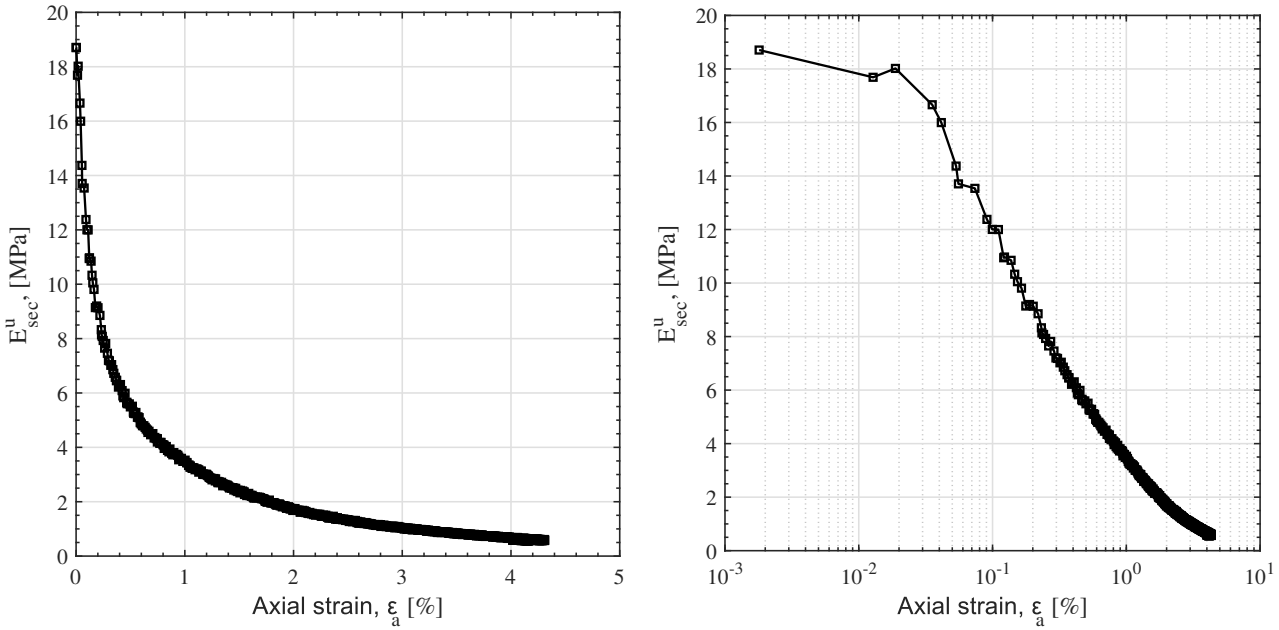


(d) $q_{mean} = 47\,\text{kPa}$; $q_{cyc} = 5\,\text{kPa}$

Figure 3.6: *Evolution of undrained secant Young modulus E^u_{sec} as function of the number of loading cycles N for cyclic triaxial tests that are anisotropically consolidated to in-situ stress conditions p'_0, q_0, subsequently sheared in undrained conditions to a new p', q_{mean} before undrained cyclic loading with q_{cyc}. Note that the test with $q_{cyc} = 5\,\text{kPa}$ did not fail during cyclic loading.*

E^u_{sec} for monotonic shearing

A baseline result for the undrained secant stiffness E^u_{sec} for a monotonically sheared test is shown in Fig. 3.7. This is the reference anisotropically consolidated undrained triaxial compression test (CAUC) on a sample from a depth of 9 m. Please note that whilst the test is sheared to failure at large magnitudes of axial strain, Figs. 3.7a & 3.7b only show the axial strains ε_a up to just over 4%. The semi-logarithmic scale in Fig. 3.7b elucidates the rapid drop in the magnitude of the E^u_{sec}.



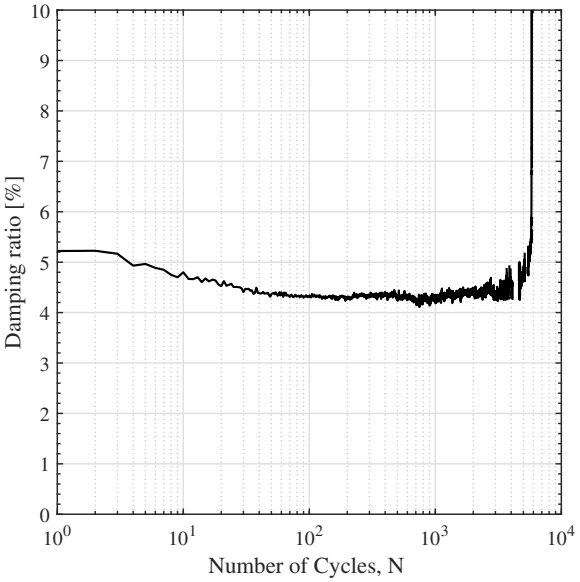
(a) *Linear scale.* (b) *Logarithmic scale.*

Figure 3.7: E^u_{sec} *from reference CAUC test; Test 01.*

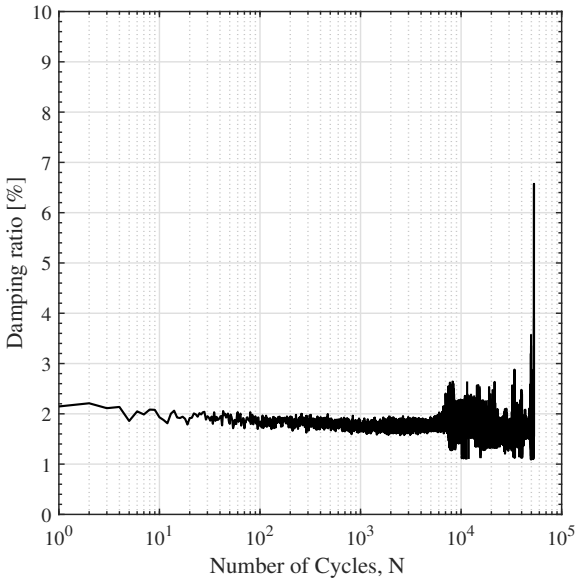
3.3.3 Damping ratio

Without pre-shearing

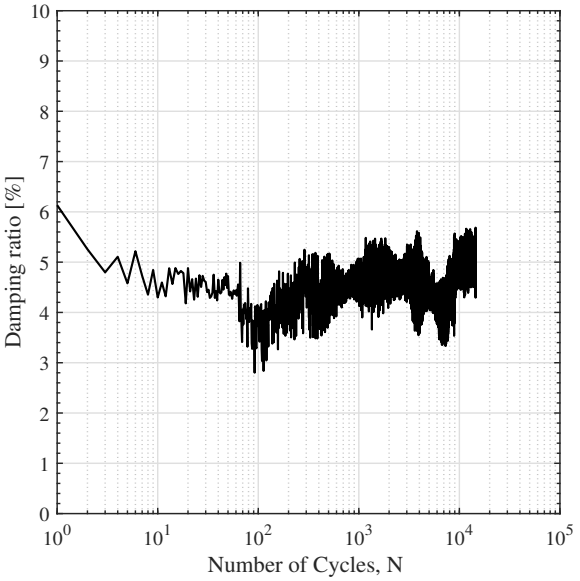
Fig. 3.8 plots the evaluated damping ratio for the same tests, and in the same order, as presented in Fig. 3.5, *i*.e., those directly tested after anisotropic consolidation to *in-situ* conditions. The damping ratio seems rather stable, regardless of loading amplitude q_{cyc}, further discussion are presented in Section 3.3.5.



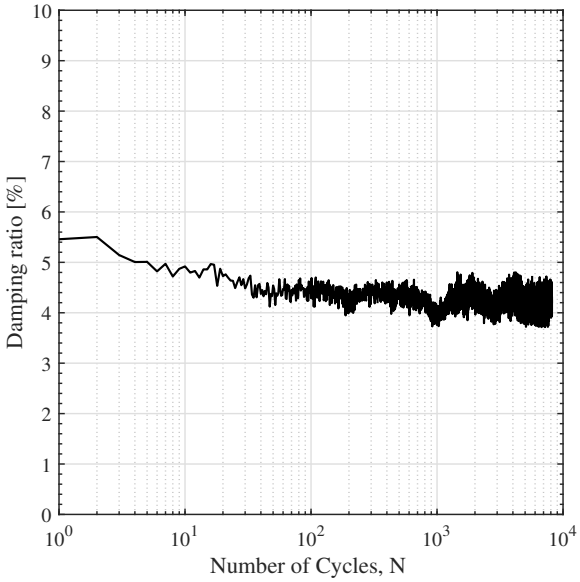
(a) $q_{mean} = 28\,\text{kPa}$; $q_{cyc} = 28\,\text{kPa}$



(b) $q_{mean} = 28\,\text{kPa}$; $q_{cyc} = 20\,\text{kPa}$



(c) $q_{mean} = 28\,\text{kPa}$; $q_{cyc} = 10\,\text{kPa}$

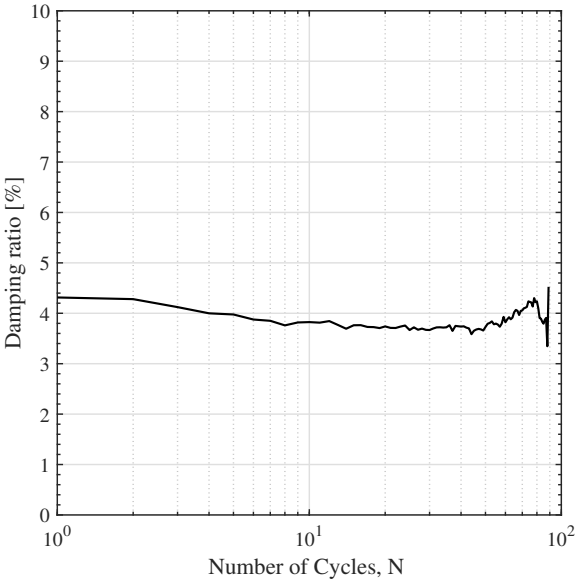


(d) $q_{mean} = 28\,\text{kPa}$; $q_{cyc} = 5\,\text{kPa}$

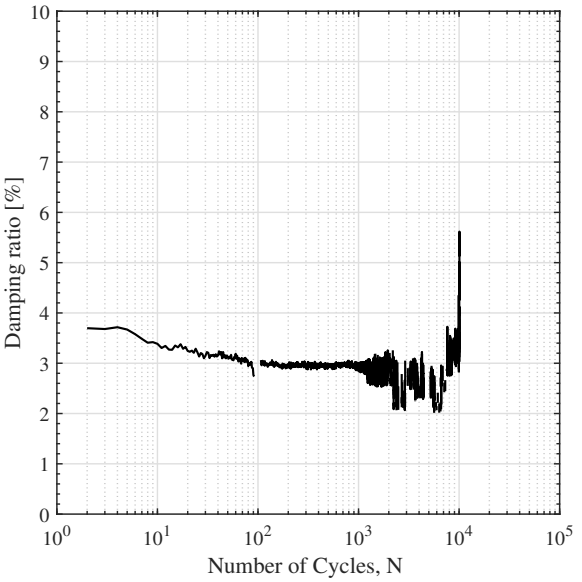
Figure 3.8: *Evolution of damping ratio as function of the number of loading cycles N for cyclic triaxial tests that are anisotropically consolidated to* in-situ *stress conditions* p'_0, q_0 *before undrained cyclic loading with* q_{cyc}. *Note that the tests with* $q_{cyc} = 5$ *&* $10\,\text{kPa}$ *did not fail during cyclic loading.*

With pre-shearing

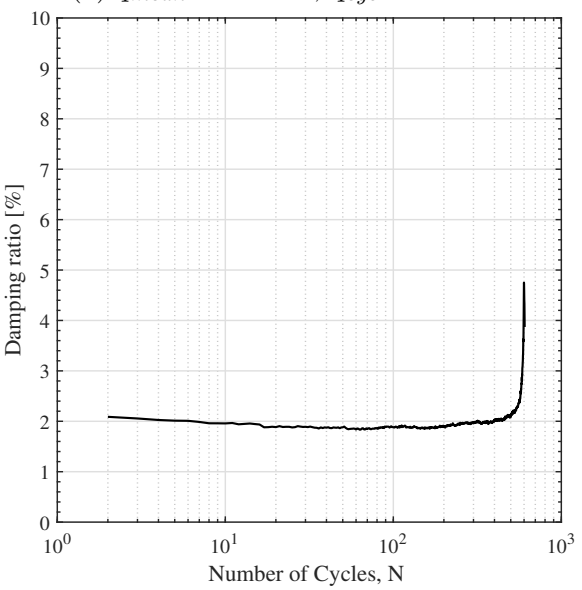
Fig. 3.9 plots the evaluated damping ratio for the same tests, and in the same order, as presented in Fig. 3.6, *i*.e., those tested after undrained pre-shearing (in loading and/or unloading) of anisotropically consolidated samples. For these tests the damping ratio seems to be affected by the pre-shearing in compression, *i*.e., $q_{mean} = 37\,\text{kPa}$ & $47\,\text{kPa}$, irrespective of loading amplitude q_{cyc} an increased q_{mean} seems to relate to a reduced damping ratio. The results are elaborated further in Section 3.3.5.



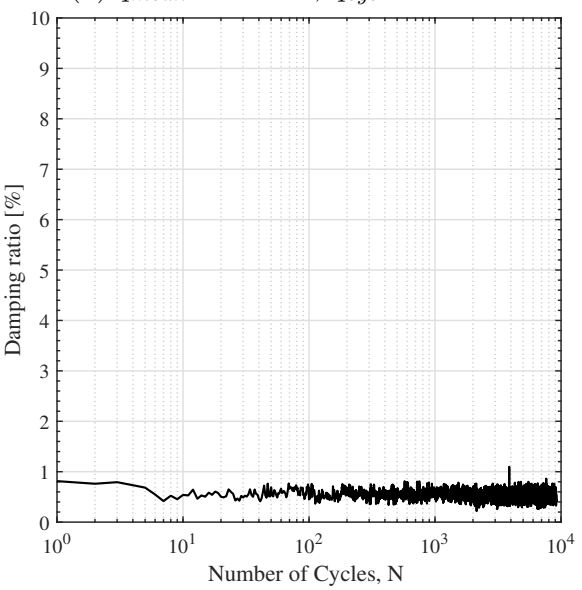
(a) $q_{mean} = 20\,\text{kPa}$; $q_{cyc} = 38\,\text{kPa}$



(b) $q_{mean} = 10\,\text{kPa}$; $q_{cyc} = 29\,\text{kPa}$



(c) $q_{mean} = 37\,\text{kPa}$; $q_{cyc} = 20\,\text{kPa}$

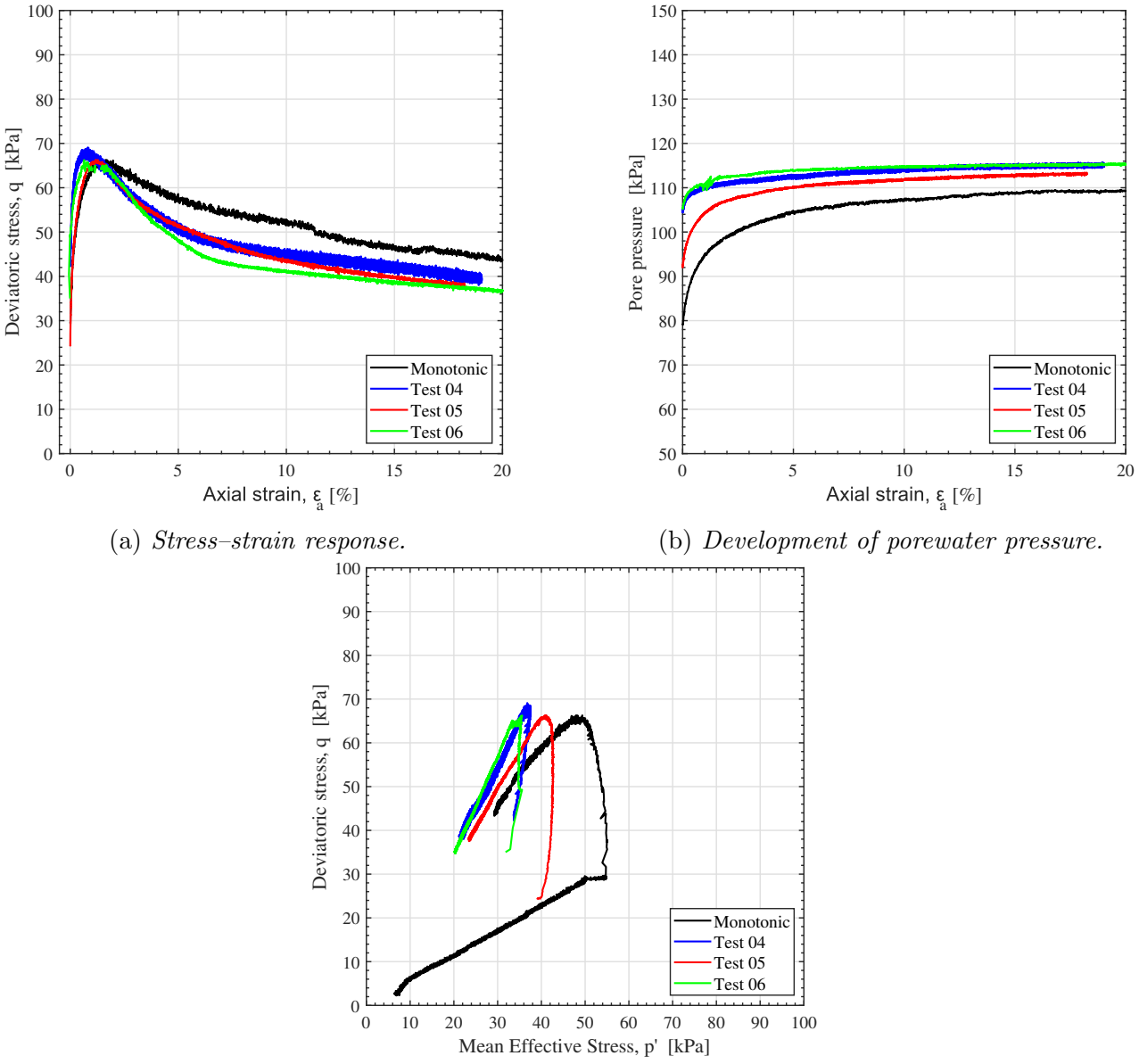


(d) $q_{mean} = 47\,\text{kPa}$; $q_{cyc} = 5\,\text{kPa}$

Figure 3.9: *Evolution of damping ratio as function of the number of loading cycles N for cyclic triaxial tests that are anisotropically consolidated to* in-situ *stress conditions* p'_0, q_0, *subsequently sheared in undrained conditions to a new* p', q_{mean} *before undrained cyclic loading with* q_{cyc}. *Note that the test with* $q_{cyc} = 5\,\text{kPa}$ *did not fail during cyclic loading.*

3.3.4 Post-cyclic shearing

Three tests did not fail during the cyclic loading stage, due to the small cyclic deviatoric loading amplitudes applied. The prematurely aborted tests were subsequently sheared in undrained conditions. A comparison between the results of an ordinary CAUC test performed on a sample from the same depth and the three post-cyclically sheared tests is shown in Figure 3.10. Clearly, cyclic loading has only a small impact on the emerging undrained shear strength ($s_u = q/2$), *e.*g., 3.10a. As well as that despite the shift in excess porewater pressures from pre-shearing and cyclic loading 3.10b, also the stress ratio at critical state seems not to change, as can be witnessed from Fig. 3.10c.



(a) *Stress–strain response.*

(b) *Development of porewater pressure.*

(c) *Stress paths.*

Figure 3.10: *Undrained shearing stage for reference CAUC test and three post-cyclic shearing stages. Tests 4 (pre-sheared) & 5 were cyclically loaded with* $q_{cyc} = 5\,\mathrm{kPa}$ *and test 6 with* $q_{cyc} = 10\,\mathrm{kPa}$.

3.3.5 Discussion of results

Cyclic response without undrained pre-shearing

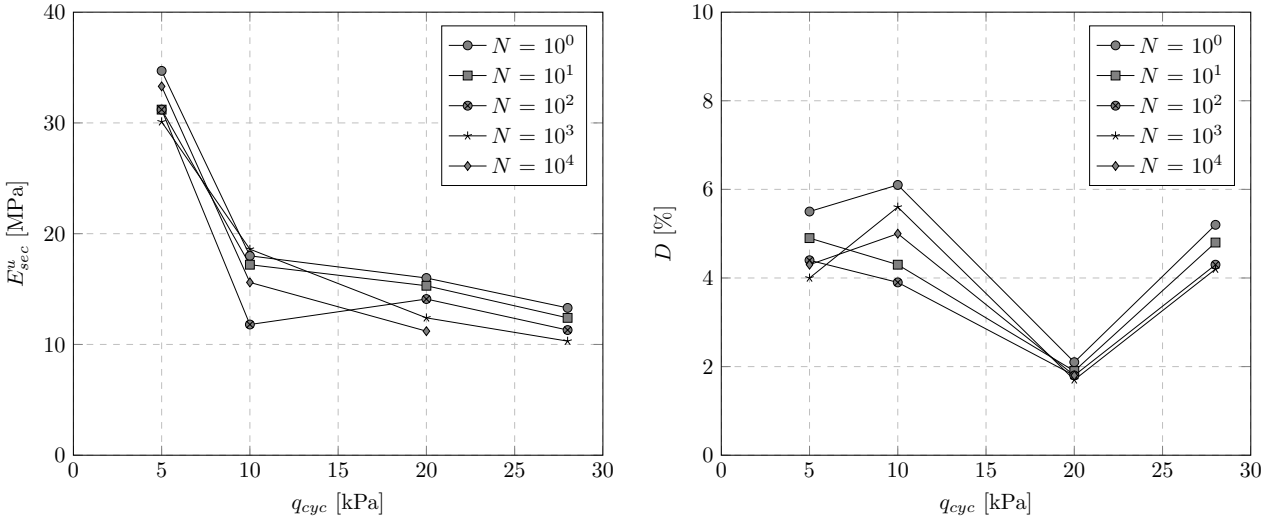
For the tests that are consolidated to the *in-situ* conditions without pre-shearing, the interpreted cyclic data is aggregated in Figure 3.11 for the undrained secant stiffness and the damping ratio. This comparison is not as is easily made when pre-shearing data needs to be included, as in those tests both the pre-shearing and the cyclic loading amplitude are changed.

The magnitude for the undrained secant stiffness E^u_{sec} presented in Fig. 3.11a is ranging between 18 and 13 MPa for cyclic loading amplitudes over q_{cyc} 10 kPa ($> 0.15{*}s_u$), corresponding to an axial strain amplitude in the range $5\text{x}10^{-4}$ and $2\text{x}10^{-3}$. This is comparable to the undrained secant stiffness of $\approx$ 18 MPa found at magnitude of 10^{-4} axial strain in the monotonic reference test presented in Fig. 3.7b.

The undrained secant stiffness subsequently degrades with an additional 20 - 25 % as the number of cycles N reaches 10^4. The latter roughly corresponds to a stiffness reduction of 5–6 % for each tenfold increase of number of cycles.

Only for the substantially lower amplitudes of $q_{cyc} = 5$ kPa the stiffness on average doubles in magnitude, ranging between 30 and 35 MPa at a strain amplitude of $\approx 1\text{x}10^{-4}$. This value is a lower bound of the range found from *in situ* seismic measurements, reported in Wood, 2016. For this amplitude, the stiffness fluctuates without a clear downward trend, as was observed for the data at large loading amplitudes. Furthermore, for large loading amplitudes, *i*.e., q_{cyc} > 20 kPa the maximum number of loading cycles until failure is reached between 10^3 and 10^4 cycles, whereas for the other loading amplitudes no failure was detected.

The overview for the damping ratio D is less clear, with the test conducted at $q_{cyc} = 20$ kPa clearly showing the least damping at 2 %, which might be due to the specific sample tested. The other tests show very comparable results in the range of 4–6 %, where the reduction in damping with the number of loading cycles is not consistent and test specific, *i*.e., the majority of tests show an initial reduction of damping that subsequently is recovered.



(a) E^u_{sec}. (b) *Damping ratio D.*

Figure 3.11: *Overview of degradation of undrained secant stiffness* E^u_{sec} *and damping ratio D as function of cyclic loading amplitude* q_{cyc} *and number of cycles N. All results are for Kärra samples from* 9 m *depth that are anisotropically consolidated to the in-situ stress state.*

Cyclic response with undrained pre-shearing

The impact of pre-shearing, *i*.e., varying q_{mean} in a monotonic undrained loading path prior to cyclic loading, on the emerging stiffness and damping ratio is pronounced. The number of cycles towards failure reduces substantially with an additional undrained pre-cyclic shearing stage (think of embankment loading or excavation).

Due to choosing pairs of q_{mean} and q_{cyc} that preserve a constant factor of safety FS (see Fig. 3.2), the comparisons for the tests with pre-shearing are not as straight-forward. The combination of a lower q_{mean} with increased q_{cyc} fails faster than the test with a comparable safety factor that is realised by increasing q_{mean} yet reducing q_{cyc}. This finding is illustrated by comparing test 11 in Fig. 3.6a (failure at $N = 70$ cycles) and test 08 in Fig. 3.6c (failure at $N = 580$ cycles). However, for both cases pre-shearing is detrimental when compared to the reference case without pre-shearing, *i*.e., test 09 in Fig. 3.5a that fails after $N = 5800$ cycles. The additional excess porewater pressures that are generated in the undrained unloading/loading stage prior to shearing substantially reduce the cyclic loading capacity of the clay.

The damping ratio D for all pre-sheared tests shows a clear reduction for tests that were pre-sheared in undrained conditions towards a q_{mean} above the original in-situ $q_{mean} = q_0 = 28\,\text{kPa}$. The test with $q_{mean} = 47\,\text{kPa}$ and $q_{cyc} = 5\,\text{kPa}$ resulted in a very low damping below 1 %. Unloading does not have that pronounced effects.

Post-cyclic monotonic strength

Several interesting observations are discerned when the samples are sheared after cyclic loading at small loading amplitude. The magnitude of the undrained shear strength, *i*.e., $s_u = q/2$ does not appreciably change after cyclic loading with low q_{cyc} with up to $N = 10^4$ loading cycles (Fig. 3.10a). Furthermore, all tests seem to have reached critical state as the excess porewater pressures stabilise at large magnitudes of axial strain (Fig. 3.10b).

During the shearing stage the generation of excess porewater pressures is more limited for the cyclic tests when compared to the monotonic test (Fig. 3.10b). However, the tests with pre-shearing and $q_{cyc} = 5\,\text{kPa}$ and no pre-shearing with $q_{cyc} = 10\,\text{kPa}$ accumulated the highest excess porewater pressures prior to the shearing stage. The stress paths indicate that, neither the undrained shear strength nor the stress ratio at critical state are affected much by the cyclic loading history (Fig. 3.10c). The (limited) data suggest that the ultimate M-line for the post-cyclic data is approximately the same as for the monotonic shearing.

4 Conclusions, recommendations & impact

4.1 Conclusions

This report summarises the advances made at Chalmers on modelling and testing cyclic degradation, with a focus on the evolving stiffness and damping properties. The following main activities have been employed:

- A small-strain stiffness formulation was added for the elastic domain, *i*.e., both for Creep-SCLAY1S and Creep-SCLAY1Sc.

- Local instrumentation was found to affected by membrane weakening, when paraffin oil is used as cell liquid.

- The execution of an extensive programme of cyclic triaxial tests that investigated the impact of loading amplitude and undrained pre-shearing on the subsequent cyclic response of sensitive clay was described.

The results can be summarised as:

- For samples consolidated to the the *in situ* stress state that are cyclically loaded in undrained conditions with medium to large loading amplitudes, *i*.e., $q_{cyc} > 10\,\text{kPa}$ (which corresponds to 15% the undrained shear strength), the undrained secant stiffness corresponds to that of a monotonically loaded test. This value further reduces with 5% per decade upon cyclic loading at a loading period of 120 s until failure. Large loading amplitudes lead to earlier failure.

- In the current tests the 'small-strain' stiffness from undrained loading with 5 kPa cyclic loading amplitude at an average strain level of 10^{-4} is $\approx$ two times of that found for larger loading amplitudes or monotonic shearing. It should be noted that this strain magnitude is still higher than obtained from seismic measurements, yet compares well to the lower bound of *in situ* seismic measurements from the Gothenburg area.

- The results of the post-cyclic shearing of the samples that did not fail during cyclic loading up to 10^4 cycles, *i*.e., those with small loading amplitudes $< 10\,\text{kPa}$ indicate that the undrained strength is not affected.

- An undrained unloading has a larger impact on the subsequent cyclic response than undrained loading. In both cases pre-shearing reduced the cyclic capacity of the samples tested.

- The damping ratio is relatively stable at 5% for most samples tested, without significant impact of the number of loading cycles, amplitude. Undrained pre-shearing has the largest impact on the damping ratio.

4.2 Recommendations

- Adding an undrained stress-controlled loop with loading amplitude below 5 kPa or $\approx 0.075 s_u$ (in compression) as part of a standard anisotropically loaded undrained shear test in compression would give valuable information on the 'small strain' shear stiffness without the need of additional seismic instrumentation. This requires adequate external instrumentation that is validated against local instruments.

- The degradation of dynamic properties in a sensitive clays below railway systems are largely linked to a change in stiffness, without an appreciable difference in the damping ratio. Furthermore, the undrained shear strength seems not be affected.

- The results should be expanded with complementary tests on deep-mixed clays, as those comprise most of the contemporary railway foundations on soft clays. This includes linking the laboratory based measurements with observations from *in situ* techniques.

4.3 Impact

The results of the project have had both direct and indirect impact. The small-strain extension of Creep-SCLAY1S will be used in BIG project A2021-06 for the analyses of deep excavations, whereas the reformulated Creep-SCLAY1Sc model for small strain will be further calibrated against the data reported herein before a detailed numerical sensitivity study as part of a PhD project at Chalmers. In turn, this sensitivity study will form the base for subsequent Data Assimilation strategies for monitoring data on railway infrastructure. Those algorithm are already under development in FORMAS project 2020-00220.

Furthermore, the experimental equipment, procedures and scripts for interpretation, will directly be used for testing deep mixed clays in the follow-on BIG project A2021-20.

In addition, some of the knowledge developed finds its way into CHARMEC project TS-22 (PI Prof. Jens Nielsen).

As such, the funding has contributed towards several on-going and follow up activities that ultimately will contribute to the proactive maintenance of physical linear infrastructure.

References

Bishop, A.W. and L.D. Wesley (1975). A hydraulic triaxial apparatus for controlled stress path testing. *Géotechnique* **25**.4, 657–670 (cit. on p. 5).

Dijkstra, J. and H. Tahershamsi (2020a). *Dynamic response of a transition zone on soft clay*. Tech. rep. Chalmers University of Technology, Sweden (cit. on p. 1).

Dijkstra, J. and H. Tahershamsi (2020b). *Modelling deformations below high-speed rail*. Tech. rep. Chalmers University of Technology, Sweden (cit. on p. 1).

Karstunen, M. and J. Dijkstra (2021). *A2014-14 Final report for project: On the fundamental relation between soil creep and cyclic pile-soil response*. Tech. rep. Chalmers University of Technology, Sweden (cit. on pp. 1, 5).

Powrie, William, Louis Le Pen, David Milne, and David Thompson (2019). Train loading effects in railway geotechnical engineering: Ground response, analysis, measurement and interpretation. *Transportation Geotechnics* **21**, 100261 (cit. on p. 1).

Sivasithamparam, N., M. D'Ignazio, A.B. Tsegaye, J. Castro, and C. Madshus (2021). "Small strain stiffness within logarithmic contractancy model for structured anisotropic clay". *IOP Conference Series: Earth and Environmental Science*. Vol. 710. 1. IOP Publishing, p. 012042 (cit. on p. 4).

Wichtmann, T. (2005). "Explicit accumulation model for non-cohesive soils under cyclic loading". PhD thesis. Ruhr-University Bochum (cit. on p. 1).

Wichtmann, T., K.H. Andersen, M.A. Sjursen, and T. Berre (2013). Cyclic tests on high-quality undisturbed block samples of soft marine Norwegian clay. *Canadian Geotechnical Journal* **50**.4, 400–412 (cit. on p. 3).

Wood, T. (2016). "On the Small Strain Stiffness of Some Scandinavian Soft Clays and Impact on Deep Excavations". PhD thesis. Chalmers University of Technology (cit. on p. 17).

Zuada Coelho, Bruno, Jelke Dijkstra, and Minna Karstunen (2021). Viscoplastic cyclic degradation model for soft natural soils. *Computers and Geotechnics* **135**, 104176 (cit. on pp. 1, 3).

BIG – Branschsamverkan i grunden
Forskningsprogram för effektiv och säker grundläggning av vägar och järnvägar

BIG

BIG – Branschsamverkan i grunden - är ett forskningsprogram för effektiv och säker grundläggning av transportsystemets infrastruktur. Programmet etablerades under senhösten 2013, och påbörjade sin verksamhet den 1 januari, 2014.

Målsättningen är att sänka kostnader för byggande och underhåll av transportsystemets infrastruktur genom ett långsiktigt och systematiskt utvecklingsarbete inom geoteknikområdet.

I BIG samverkar Trafikverket, Chalmers tekniska högskola, Luleå tekniska universitet, Kungliga tekniska högskolan och Statens geotekniska institut.

Resultat från BIG projekt publiceras i vetenskapliga artiklar och parternas egna rapportserier. Alternativt så publiceras rapporterna i denna gemensamma BIG rapport serie.

Publicerade rapporter

A2014:03	Deformationer i undergrund – Litteratursammanställning och analys
A2014:07	Grundvattensänkning i morän
A2014:13	Höghastighetsspår i Sverige – på bank
A2014:14	On the fundamental relation between soil creep and cyclic pile-soil response
A2016:05	Modelling deformations below high-speed rail
A2017:07	Dynamic response of transition zone on soft clay
A2017:10	Effects of climate change on slopes in sensitive clay
A2017:14	Changes in undrained shear strength as a function of time under embankments
A2018:03	Three-dimensional effects in slope stability calculations
A2018:18	Osäkerhetsmodeller – för optimal geoteknisk resusanvändning.
A2018:22	Towards high quality deep soft soil samples
A2019:02	Degradation of a natural sensitive clay under cyclic loading
A2020:08	Towards contemporary erosion solutions